Available online at www.sciencedirect.com

ScienceDirect

Procedia Structural Integrity 80 (2026) 212–218

Structural Integrity Procedia

www.elsevier.com/locate/procedia

Fracture, Damage and Structural Health Monitoring

Predicting the Deformation Behavior of Biocomposites using Combined Mathematical and AI-Based Modeling

Thierry Barriere[a], Vincent Placet[a], Sami Holopainen[a,b,*], Ndeye Niang[a]

[a]Marie and Louis Pasteur University, SUPMICROTECH-ENSMM, CNRS, Institute FEMTO-ST, F-25000 Besancon, France.
[b]Tampere University, Department of Civil Engineering, FI-33014 Tampere, Finland.

Abstract

The use of fossil plastic materials is being significantly replaced by renewable raw materials, such as natural short fiber reinforced (NSFR) polymer composites (biocomposites). Due to the increasing popularity of biocomposites nowadays, ranging from their applications in the food packaging to automotive and aerospace industry, volume of their experimental research is huge. However, experimental research is costly and time consuming. In this research, a micromechanically based constitutive model is proposed to investigate and simulate the elastic-viscoplastic and micro- to macro-scopic deformation behavior of the biocomposites consisting of short biofibers (hemp) and a semi-crystalline polymer matrix (PLA). However, also the constitutive mathematical modeling as such is computationally time-consuming when applied to predict long-term deformation behavior in large design spaces. Therefore, a combination of the proposed mathematical model and an AI-model is proposed. Idea of the concept is that the mathematical model is solely used to predict high-quality data for machine learning (ML) which is computationally very efficient.

Keywords: Biocomposite; modeling & experimentation; plasticity; artificial intelligence (AI); digital twins

1. Introduction

The experimentation of materials and their deformation under various loads is costly and time-consuming and therefore, the motivation of model predictions is that they can rapidly and systematically scan a vast number of material grades, manufacturing steps, and loading conditions. Despite this motivation, research volume in modeling and simulation of mechanical behavior of biocomposites, such as NSFR polymer composites, is limited; those composites have huge application potential because the variation of the plastic matrix combined with different plant fibers (hemp, cotton, flax, jute, ramie, conifer, bagasse) is almost unlimited and they are applied e.g., in automotive and aeronautic industry, health technology, and electronic devices Ning et al. (2012); Naili et al. (2020).

* Corresponding author.
E-mail address: sami.holopainen@tuni.fi

10.1016/j.prostr.2026.02.021

Many capable constitutive models of predicting nonlinear stress vs strain (σ vs ϵ) response are based on an assumption of nonlinear (visco)elasticity Naili et al. (2020); Chandekar et al. (2022); Wang et al. (2023) or the response is elastic-fully plastic Andersons et al. (2016). Some studies suggest the application of the inelastic Ramberg-Osgood or alternatively Drucker–Prager models Modniks and Andersons (2013); Notta-Cuvier et al. (2013). However, these models have not a clear connection to the microstructural behavior and their predictions lack to represent long-term viscous deformation, such as stress relaxation, creep, and recovery at nearly zero stress.

The models for fiber-reinforced polymers can be classified to mean-field models and full-field models Modniks and Andersons (2013); Hessman et al. (2021); Dey et al. (2023); Praud et al. (2024). In the mean-field models, average strain and stress of a micro- or macro-structure represent the real nano- or micro-scopic strain and stress, when a homogenization step is required Jeulin and Forest (2024). However, in addition to complex parameter calibration, homogenization of the stress field depending on the fiber orientation affects inaccuracy. In contrast to mean-field models, full-field models account for microscopic fields at microscopic points and they require realistic Representative Volume Elements (RVEs) representative for the micro-structure Naili et al. (2020); Hessman et al. (2021); Praud et al. (2024); Jeulin and Forest (2024). However, the notable fiber volume fractions and aspect ratio (AR), generating of realistic RVEs, are challenging and cause high computational costs when applied to macroscopic deformation scale for real engineering design.

Here, a compact viscoelastic-plastic constitutive model (mean-field) for NSFR semi-crystalline polymers is proposed. While a number of internal variables and model parameters was reduced, the model can predict the effect of the fiber content, degree of crystallization (DC), and porosity being therefore capable of reproducing dilatation-caused microstructural changes. Advantages of this compact end-to-end model are the realistic viscoelastic-plastic predictions in creep, nonlinear unloading, and stress relaxation attained by a minimum set of variables and parameters compared to previous capable models.

However, the constitutive mathematical modeling is challenging and computationally time-consuming when applied in large-design spaces and to predict long-term behavior, particularly fatigue Barriere et al. (2020, 2021). Therefore the mathematical models are increasingly being replaced by more efficient meta-models based on AI and ML, because they only require high-quality data Yang et al. (2018); Zhai et al. (2020); Laycock et al. (2024); Lu et al. (2025). This work combines the benefits of the conventional mathematical modeling and the AI-based modeling: missing experimental data for ML is replaced by the predicted, high-quality model data.

2. Modeling

For the investigation of plastically deformable (ductile) composites (near RT), the model was based on the split of the deformation gradient (in the position $\boldsymbol{X}$ at the time t) into the elastic and viscoelastic-plastic parts: $\boldsymbol{F} = \boldsymbol{F}^{\mathrm{e}}\boldsymbol{F}^{\mathrm{vep}}$ ($\boldsymbol{F}(\boldsymbol{X}, t = 0) = \mathbf{1}$), where $\boldsymbol{F}^{\mathrm{e}}$ and $\boldsymbol{F}^{\mathrm{vep}}$ determine the local deformations resulting from elastic and viscoelastic-plastic mechanisms, respectively Barriere et al. (2019). The deformation of plant fibers (hemp) is limited and they are considered practically elastic Modniks and Andersons (2013), whereas the polymer matrix governs reversible viscoelastic deformation and irreversible viscoplastic deformation. When the DC of the matrix is sufficiently low (less than 50 %), deformation of the crystalline phase relative to the amorphous phase is small Bartczak (2017)(Fig. 2) and it can be assumed elastic without a marked error in the total deformation. Furthermore, due to the strong bonding between the fibers and matrix and the very high strength and limited (elastic) deformability of the fibers relative to the matrix, the crystalline phase and the elastic portion of the amorphous phase deform averagely (microstructurally) in accordance with the fibers; the applied fiber length is ~160 μm which is magnitudes longer than those of amorphous chain lengths and dimension of the crystalline regions, ~100 nanometers Corneilliea and Smet (2015). Then the elastic deformation of matrix obeys the elastic deformation of fibers, and the compatibility condition $\boldsymbol{F}^{\mathrm{c}} = \boldsymbol{F}^{\mathrm{e,a}} = \boldsymbol{F}^{\mathrm{f}} = \boldsymbol{F}^{\mathrm{e}}$ (c=crystalline, a=amorphous, f=fiber) is relevant. The rheology of the model is demonstrated in Fig. 1. The average macroscopic stress in the fibers is given by

$$\boldsymbol{\sigma}^{\mathrm{f}} = \xi\mathfrak{L}^{e,f} : \ln\boldsymbol{v}^{\mathrm{e}} = \xi E^{\mathrm{f}}/[3(1-2\nu^{\mathrm{f}})]\mathrm{tr}\,(\ln\boldsymbol{v}^{\mathrm{e}})\boldsymbol{i} + \xi E^{\mathrm{f}}/(1+\nu^{\mathrm{f}})\ln\boldsymbol{v}^{\mathrm{e}}, \tag{1}$$

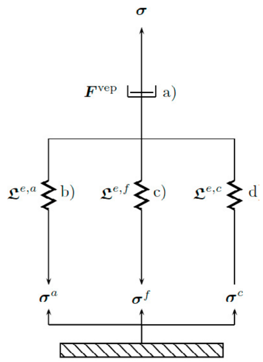

Fig. 1. Rheological representation of the microstructure-based model. Viscoelastic-plastic deformation of the amorphous phase is described by $\boldsymbol{F}^{\mathrm{vep}}$ and a single nonlinear dashpot a). The elastic deformation $\boldsymbol{F}^{\mathrm{e}}$ consisting of the elastic deformation of the amorphous phase, the fiber deformation, and the deformation of the crystalline phase are described by the elastic springs b), c), and d), respectively.

where ξ is the fiber content (%wt), E^{f} is the Young's modulus, ν^{f} is the Poisson's ratio, the notation tr denotes the tensor trace, and $\boldsymbol{\nu}^{\mathrm{f}} = \boldsymbol{\nu}^{\mathrm{e}} = \boldsymbol{F}^{\mathrm{e}}\boldsymbol{F}^{\mathrm{e,T}}$ Holopainen and Barriere (2018). If the fiber orientation after manufacturing shows a notable orientation (the Young's modulus and the Poisson's ratio show notable differences in main directions), one needs to replace the elastic stiffness tensor $\mathfrak{L}^{e,f}$ in (1) by the orthotropic or ransversally isotropic one.

The crystalline phase shows an anisotropy due to the alignments of the crystalline regions. However, in micro- to macro-level, crystalline regions are randomly arranged and their significance in relation to the fibers is small. Therefore, the anisotropic effect of crystalline regions can be omitted and the average macroscopic stress over crystalline regions is

$$\boldsymbol{\sigma}^{\mathrm{c}} = (1-\xi)\mathfrak{L}^{e,c} : \ln \boldsymbol{\nu}^{\mathrm{e}} = (1-\xi)E^{\mathrm{c}}/[3(1-2\nu^{\mathrm{c}})]\mathrm{tr}\,(\ln \boldsymbol{\nu}^{\mathrm{e}})\boldsymbol{i} + (1-\xi)E^{\mathrm{c}}/(1+\nu^{\mathrm{c}})\ln \boldsymbol{\nu}^{\mathrm{e}}, \tag{2}$$

where ν^{c} is the Poisson's ratio of crystalline regions and E^{c} is the corresponding Young's modulus with the relations [a] $(1-\zeta)E^{\mathrm{m}} = \chi E^{\mathrm{c}} + (1-\chi)(1-\zeta)E^{\mathrm{a}}$ and [b] $E = \xi E^{\mathrm{f}} + (1-\xi)(1-\zeta)E^{\mathrm{m}}$, where $0 < \chi \leq 0.5$, $\zeta < 0.1$, $\xi > 0.2$, E^{m}, E^{a}, and E^{f} are the DC, porosity, fiber content, and the Young's moduli of the matrix, its amorphous phase, and the fibers, respectively. Therefore, it is necessary to measure the Young's modulus of the composite E, matrix E^{m}, and its amorphous phase E^{a} only, whereas the E^{c} and E^{f} are calculated from the relations [a] and [b].

The viscoelastic-plastic component $\boldsymbol{F}^{\mathrm{vep}}$ in the decomposition manifests as macroscopic nonlinear monotonic loading, long-term creep strain, stress relaxation, and nonlinear unloading response owing to the inertia of the nano-microstructure to attain its equilibrium, and it is calculated as $\dot{\boldsymbol{F}}^{\mathrm{vep}} = \bar{\boldsymbol{D}}^{\mathrm{vep}}\boldsymbol{F}^{\mathrm{vep}}$, where $\bar{\boldsymbol{D}}^{\mathrm{vep}}$ is the viscoelastic-plastic rate of deformation. As a departure from the previous theories for polymers, Anand and Ames (2006); Barriere et al. (2019, 2021), the $\bar{\boldsymbol{D}}^{\mathrm{vep}}$ is the sum of several micromechanisms. However, noting the restricted deformability of NSRF polymers, a single micromechanism (a single nonlinear dashpot in Fig. 1) is considered to be sufficient to reproduce nonlinear σ vs ϵ response, when

$$\bar{\boldsymbol{D}}^{\mathrm{vep}} = (\dot{\gamma}^{\mathrm{vep}}/(2\tau) - 1/\eta)\boldsymbol{\sigma}^{\mathrm{dev}}, \tag{3}$$

where $\tau = \sqrt{1/2\mathrm{tr}\,(\boldsymbol{\sigma}^{\mathrm{dev}})^2}$. The constant viscosity η is used for capturing stress relaxation and creep, and it is constrained by the relation $\dot{\gamma}^{\mathrm{vep}}/(2\tau) - 1/\eta \geq 0$ ($\eta \sim 10^4$ MPas) and otherwise, $\bar{\boldsymbol{D}}^{\mathrm{vep}} = \boldsymbol{0}$. Without this term, the proposed Maxwell-like model shown in Fig. 1 would result in too melt fluid at RT. The evolution of viscoelastic-plastic deformation is modeled by the power-law type strain rate Anand and Ames (2006):

$$\dot{\gamma}^{\mathrm{vep}} = \left(\frac{\tau}{s^{\mathrm{a}} - 1/3\varsigma I_1}\right)^{1/m}\dot{\gamma}_0^{\mathrm{a}} \geq 0, \tag{4}$$

where $\dot{\gamma}_0^{\mathrm{a}}$, m (the limit $m \to 0$ corresponds to the rate-independency), and ς denote the material parameters, s^{a} is an internal state variable (the resistance to plastic shear flow Anand and Ames (2006); Holopainen (2013, 2014)) and I_1 is the first stress invariant indicating pressure: plastic deformation is suppressed under compression, i.e., micro-cracks are opened in tension and partly closed in compression. Therefore, the proposed plastic flow evolution (4) results in the observed asymmetry between compression and tension Anand and Ames (2006); Cherouat et al. (2018); Barriere et al. (2020). Finally, the stress of the isotropic amorphous phase is given by

$$\boldsymbol{\sigma}^{\mathrm{a}} = (1-\xi)\mathfrak{L}^{e,a} : \ln \boldsymbol{v}^{\mathrm{e}} = (1-\xi)E^{\mathrm{a}}/[3(1-2\nu^{\mathrm{a}})]\mathrm{tr}\,(\ln \boldsymbol{v}^{\mathrm{e}})\boldsymbol{i} + (1-\xi)E^{\mathrm{a}}/(1+\nu^{\mathrm{a}})\ln \boldsymbol{v}^{\mathrm{e}}, \tag{5}$$

where E^{a} is the Young's modulus and ν^{a} is the Poisson's ratio. In summary, the macroscopic viscoelastic-plastic deformation response (σ vs ϵ) is modeled by the minimum number of internal variables and parameters.

The composite test specimens (PLA + hemp 20 % + PEG plasticizers 0 - 5 wt%) were manufactured by the 3D-printing with the pellet-based material extrusion (P-MEX). The model parameters were extracted from the uniaxial monotonic tensile test results at RT (σ vs ϵ response). Moreover, the crystalline (DC > 38 %) and a virtually amorphous PLA-matrices for the Young's moduli E^{m} and E^{a} were separately investigated. The $E^{\mathrm{f}} \approx 8,100$ MPa for the hemp fiber was calculated based on the relations [a] and [b], representing an average modulus between the three main directions Placet et al. (2012). The Poisson's ratios of the different phases and the fibers were considered to be unified, $\nu^{\mathrm{f}} = \nu^{\mathrm{c}} = \nu^{\mathrm{a}} = \nu$. The applied model parameters are given in Table 1.

3. Results

The viscoplastic logarithmic strain governs the total deformation as demonstrated in Fig. 2(left); the elastic strain limit $\epsilon^{\mathrm{e}} \sim 0.004$ is also demonstrated. The predictions of monotonic loadings could be apparently improved by neglecting the brittle composite without the plasticizers. Noteworthy is the high non-linearity of the responses at small strains 0.5 - 3 %. Moreover, the observed ultimate tensile strength $\sigma_{\mathrm{u}} \sim 40$ MPa is typical for the PLA-hemp composites Ilyas et al. (2021), and the predicted nonlinear unloading response is typical for amorphous and semi-crystalline polymers Dreistadt et al. (2009); Holopainen and Wallin (2012); Holopainen (2013).

In addition, any capable model is required to provide reasonable predictions of creep and stress relaxation at different stress and strain levels, respectively. Fig. 2(right) shows the stress relaxation at different fixed strain levels ϵ_0: stress relaxation is significant and it is a nonlinear function of the ϵ_0 applied. A comparison with the pure PLA shows that the model predictions are accurate (the PLA in the composite governs the nonlinear plastic deformation and thus, relaxation).

Predicted data vs machine learning

The discussion concerns a typical problem: there is not available much enough costly experimental data to investigate all the loading conditions in question (e.g., high stress relaxation in Fig. 2(right)). It is suggested that the missing experimental data are replaced by the predicted high-quality model data which are retrieved from the advanced miscrostructural-based model proposed (calibrated to the available experimental data). Then, all the data (experimental and predicted) are used in ML, which is computationally very efficient (solely based on data). The proposed concept is particularly applicable when predicting extremely long-term deformation behavior of creep, relaxation, and particularly of fatigue, because the prediction of those phenomena by conventional mathematical models is very time-consuming Barriere et al. (2020, 2021). Furthermore, one can efficiently build digital (numerical) twins Jose and Ramakrishna (2018) for real-life objects using the proposed combination of mathematical modeling and ML.

Table 1. Model parameters for the NSFR polymer (PLA + hemp 20 %wt + PEG plasticizer 0 - 5 %wt at RT).

Parameter	E	ν	E^{f}	E^{m}	E^{a}	$\dot{\gamma}_0^{\mathrm{a}}$	s^{a}	ς	m	η
Unit	MPa		MPa	MPa	MPa	s^{-1}	MPa			MPa·s
Value	3,600	0.37	8,100	3,200	3,000	0.004	26	0.2	0.1	40,000

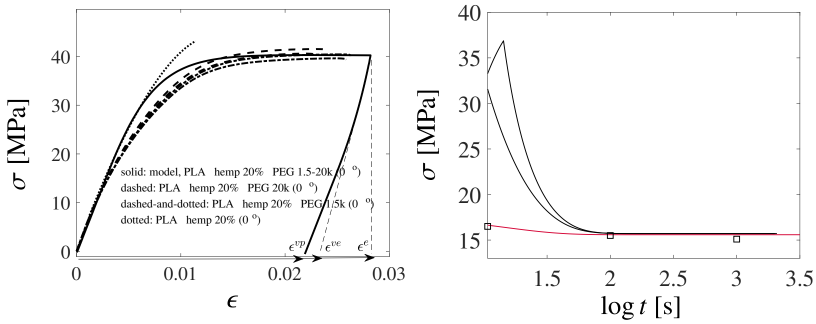

Fig. 2. Predicted (solid) and measured stress vs strain (up to rupture of the specimens; printing direction 0°) responses (left). Thin dashed straight lines demonstrate the (visco)elastic strains after unloading. Predicted stress vs time responses for the stress relaxation during one hour (right). For a comparison, data points of 3D-printed PLA (marker □ Tüfekci et al. (2023)) are also shown.

We demonstrate a reduced case, where the macroscopic deformation behavior of NSFR polymers (σ vs ϵ response) was investigated, and where the experimental data for unloading and stress relaxation were missing. The tensile stress σ (vs strain ϵ) was the goal measure for the ML to be predicted and it was shown to depend strongly and nonlinearly on the porosity, DC, and fiber content. For a ML, one needs first to investigate the correlation between the material variables mentioned. The Pearson correlation is the best known. The correlation of the material variables based on the Pearson correlation was very low (<0.012) indicating the variables are virtually independent of each other.

Due to the strong dependence of the σ vs ϵ relationship on the (independent) material variables, the selection of the suitable ML method is restricted Pedregosa and et. al. (2011); Laycock et al. (2024). Stacking is probably the most accurate and supervised (ensemble) approach because it involves training of base models (combining multiple ML models) and use of their predictions as input for meta-model predictions Pedregosa and et. al. (2011). The stacking was further reduced so that the first-level meta-model was solely based on a single base model using the SVR (based on random splitting Rivas-Perea et al. (2013)). Moreover, the first meta-model was the final model used in the final predictions. This approach was robust for the investigation of the highly nonlinear σ vs ϵ relationships, whereas unsupervised base models resulted in inaccurate predictions. The list for encoding this simple approach is:

- `Train the SVR model on the experimental and model data for the 1st meta-model (model 1)`
- `Check convergence`
- `Plot the strain vs the model 1 result (stress)`
- `Train the model 1 for the 2nd meta-model (model 2, the final meta-model)`
- `Plot the strain vs the model 2 (stress) and the experimental and predicted model data for comparison`

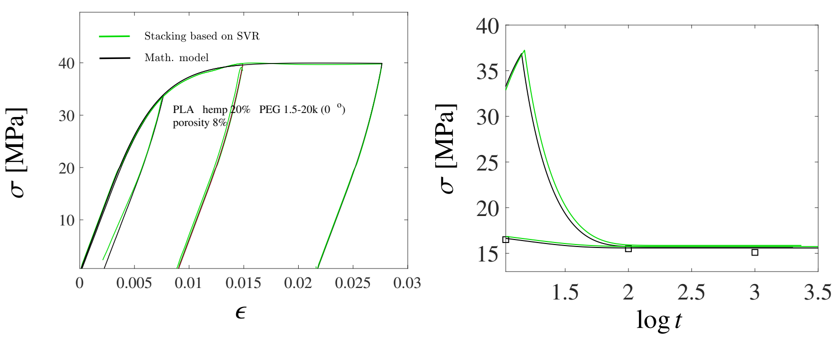

Fig. 3. Mathematical model predictions (black solid) and ML predictions [stacking based on the SVR] (green solid) (left). The mathematical model and ML predictions are partially overlapping. Predicted stress vs strain responses for the stress relaxation during one hour based on the mathematical model (black curve) and the ML predictions (green) (right). The experimental data points □ are also shown.

Fig. 3 shows the ML predictions (based on the reduced stacking) for the nonlinear loadings of the NSFR polymer (PLA + hemp 20 % + PEG 1.5 - 20k), when the porosity, DC, and fiber content were 8 %, 38 % (average value corresponding to the experimental data), and 20 %wt, respectively. For the teaching and testing of the SVR for monotonic loading, 100 % of the data was the experimental data. For unloadings, when no experimental data were available, the SVR was taught solely by the model data. For stress relaxation (including the two responses shown in Fig. 3(right)), with the scarce experimental data, the relation between the predicted and experimental data was 75 % and 25 %. Based on previous experience of the effectiveness of the SVR Pedregosa and et. al. (2011); Rivas-Perea et al. (2013) improved by stacking, it is not a surprise that the ML shows accurate predictions both for unloadings and stress relaxation because the learning was equipped with the abundant predicted model data.

Motivated by the promising results, one can assume accurate predictions by the ML (the stacking concept) also for extremely long-term deformation behavior: stress relaxation, creep, and fatigue of several years, impossible to observe experimentally nor by calculate using a mathematical constitutive model.

Acknowledgements

This work was supported by the EIPHI Graduate school (contract ANR-17-EURE-0002). The authors thank MIFHySTO and AMETISTE platforms (UFC, France) for providing test equipment. The authors thank IT Center for Science Ltd (CSC, Finland) for providing calculation resources.

References

Anand, L., Ames, N.M., 2006. On modeling the micro-indentation response of an amorphous polymer. Int. J. Plasticity 22, 1123–1170.

Andersons, J., Modniks, J., Joffe, R., Madsen, B., Nättinen, K., 2016. Apparent interfacial shear strength of short-flax-fiber/starch acetate composites. Int. J. Adhes. Adhes. 64, 78–85.

Barriere, T., Cherouat, A., Gabrion, X., Holopainen, S., 2021. Short- to long-term deformation behavior, failure, and service life of amorphous polymers under cyclic torsional and multiaxial loadings. Int. J. Plasticity 147, 103106.

Barriere, T., Gabrion, X., Holopainen, S., 2019. A compact constitutive model to describe the viscoelastic-plastic behaviour of glassy polymers: Comparison with monotonic and cyclic experiments and state-of-the-art models. Int. J. Plasticity 122, 31–48.

Barriere, T., Gabrion, X., Holopainen, S., Jokinen, J., 2020. Testing and analysis of solid polymers under large monotonic and long-term cyclic deformation. Int. J. Plasticity 135, 102781.

Bartczak, Z., 2017. Deformation of semicrystalline polymers - the contribution of crystalline and amorphous phases. Polimery 11, 785–912.

Chandekar, H., Chaudhari, V.V., Waigaonkar, S., 2022. Theoretical models for stiffness prediction of short fibre composites. Materials Today: Proceedings 57, Part 2, 711–714.

Cherouat, A., Borouchaki, H., Jie, Z., 2018. Simulation of sheet metal forming processes using a fully rheological-damage constitutive model coupling and a specific 3D remeshing method. Metals 8, 1–38.

Corneilliea, S., Smet, M., 2015. PLA architectures: the role of branching. Polymer Chemistry 6, 850–867.

Dey, A.P., Welschinger, F., Schneider, M., Gajek, S., Böhlke, T., 2023. Rapid inverse calibration of a multiscale model for the viscoplastic and creep behavior of short fiber-reinforced thermoplastics based on Deep Material Networks. Int. J. Plasticity 160, 103484.

Dreistadt, C., Bonnet, A.S., Chevrier, P., Lipinski, P., 2009. Experimental study of the polycarbonate behaviour during complex loadings and comparison with the Boyce, Parks and Argon model predictions. Materials & Design 30, 3126–3140.

Hessman, P.A., Welschinger, F., Hornberger, K., Böhlke, T., 2021. On mean field homogenization schemes for short fiber reinforced composites: Unified formulation, application and benchmark. Int. J. Solids Struct. 230-231, 111141.

Holopainen, S., 2013. Modeling of the mechanical behavior of amorphous glassy polymers under variable loadings and comparison with state-of-the-art model predictions. Mechanics of Materials 66, 35–58.

Holopainen, S., 2014. Influence of damage on inhomogeneous deformation behavior of amorphous glassy polymers. Modeling and algorithmic implementation in a finite element setting. Engng. Fract. Mech. 117, 28–50.

Holopainen, S., Barriere, T., 2018. Modeling of mechanical behavior of amorphous solids undergoing fatigue loadings, with application to polymers. Comp. Struct. 199, 57–73.

Holopainen, S., Wallin, M., 2012. Modeling of long-term behavior of amorphous glassy polymers. ASME J. Engng. Materials Technol. 135, 1–11.

Ilyas, R.A., Sapuan, S.M., Harussani, M.M., Hakimi, M.Y.A.Y., Haziq, M.Z.M., Atikah, M.S.N., Asyraf, M.R.M., Ishak, M.R., Razman, M.R., Nurazzi, N.M., Norrrahim, M.N.F., Abral, H., Asrofi, M., 2021. Polylactic Acid (PLA) Biocomposite: Processing, Additive Manufacturing and Advanced Applications. Polymers 13, 13081326.

Jeulin, D., Forest, S., 2024. Statistical approach to the Representative Volume Element Size of Random Composites. In Digital Materials: Continuum Numerical Methods at the Mesoscopic Scale. John Wiley & Sons.

Jose, R., Ramakrishna, S., 2018. Materials 4.0: materials big data enabled materials discovery. Appl Mater Today 10, 127–32.

Laycock, B.G., Chan, C.M., Halley, P.J., 2024. A review of computational approaches used in the modelling, design, and manufacturing of biodegradable and biobased polymers. Progress in Polymer Science 157, 101874.

Lu, S., Zhang, X., Hu, Y., Chu, J., Kan, Q., Kang, G., 2025. Machine learning-based constitutive parameter identification for crystal plasticity models. Mechanics of Materials 203, 105283.

Modniks, J., Andersons, J., 2013. Modeling the non-linear deformation of a short-flax-fiber-reinforced polymer composite by orientation averaging. Composites: Part B 54, 188–193.

Naili, C., Doghri, I., Kanit, T., Sukiman, M., Aissa-Berraies, A., Imad, A., 2020. Short fiber reinforced composites: Unbiased full-field evaluation of various homogenization methods in elasticity. Compos. Sci. Technol. 187, 107942.

Ning, N., Fu, S., Zhang, W., Chen, F., Wang, K., Deng, H., Zhang, Q., Fu, Q., 2012. Realizing the enhancement of interfacial interaction in semicrystalline polymer/filler composites via interfacial crystallization. Prog. Polym. Sci. 37, 1425–55.

Notta-Cuvier, D., Lauro, F., Bennani, B., Balieu, R., 2013. An efficient modelling of inelastic composites with misaligned short fibres. Int. J. Solids Struct. 50, 2857–71.

Pedregosa, F., et. al., 2011. Machine learning in python. Journal of machine learning research 12, 2825–2830.

Placet, V., Trivaudey, F., Cisse, O., Gucheret-Retel, V., Boubakar, M.L., 2012. Diameter dependence of the apparent tensile modulus of hemp fibres: A morphological, structural or ultrastructural effect? Composites: Part A 43, 275–287.

Praud, F., Schneider, K., Chatzigeorgiou, G., Meraghni, F., 2024. Microstructure generation and full-field multi-scale analyses for short fiber reinforced thermoplastics: Application to PA66GF composites. Composite Structures 341, 118175.

Rivas-Perea, P., Cota-Ruiz, J., Chaparro, D.G., Venzor, J.A.P., Carreon, A.Q., Rosiles, J.G., 2013. Support vector machines for regression: A succinct review of large-scale and linear programming formulations. Int. J. Intell. Sci. 3, 5–14.

Tüfekci, K., Çakan, B.G., Küçükakarsu, V.M., 2023. Stress relaxation of 3D printed PLA of various infill orientations under tensile and bending loadings. J. Appl. Polym. Sci. 140, 1–10.

Wang, X., Zhu, H., Song, B., Chen, X., Kennedy, D., Shi, Y., 2023. Nonlinear elastic behaviors and deformation mechanisms of nano-structured crosslinked biopolymer networks. Extreme Mechanics Letters 61, 102017.

Yang, Z., Yabansu, Y., Al-Bahrani, R., Liao, W., Choudhary, A., Kalidindi, S., Agrawal, A., 2018. Deep learning approaches for mining structure-property linkages in high contrast composites from simulation datasets. Comp Mater Sci 151, 278–87.

Zhai, C., Shi, T., Yeo, J., 2020. Discovery and design of soft polymeric bio-in-spired materials with multiscale simulations and artficial intelligence. J Mater Chem B 8, 6562–87.